

Finite-Difference Time Domain Analysis of Ultrashort Pulse Laser Light Propagation under Nonlinear Coupling*

Yoshihiko AKAMINE**, Hong Duc DOAN** and Kazuyoshi FUSHINOBU**

**Department of Mechanical and Control Engineering, Tokyo Institute of Technology
2-12-1 Ookayama, Meguro-ku, Tokyo 152-8552, Japan
E-mail: akamine.y.aa@m.titech.ac.jp

Abstract

Aim of this study is to propose a numerical model and to calculate ultrashort pulse laser light propagation by using Finite-Difference Time Domain (FDTD). "Ultrashort" pulse here is defined so that the Slowly Varying Envelope Approximation (SVEA) breaks in Beam Propagation Method (BPM) and corresponds to the pulse width of typically several tens of femtoseconds or shorter. In this case, FDTD must be used instead of BPM. In our FDTD-based model, nonlinear absorption and the effect of laser-induced plasma are newly considered unlike previously reported FDTD models. In this paper, we examine the results of FDTD-based calculation by comparing with the results of BPM-based calculation in short pulse cases where the SVEA approximation is valid. Furthermore, we calculate ultrashort pulse laser propagation and the results can describe the essential features in ultrahigh power regime.

Key words: Nonlinear Optical Effect, Ultrashort Pulse Laser, Finite Difference Time Domain, Simulation of Laser Nanomachining

1. Introduction

Development of the technologies enabled to shorten the pulse width of laser light down to sub-100-fs pulse (Stix and Ippen, 1983⁽¹⁾; DeSilvestri *et al.*, 1983⁽²⁾) and sub-10-fs pulse (Karasawa *et al.*, 2001⁽³⁾; Yamane *et al.*, 2003⁽⁴⁾). These pulse lasers have characteristics of ultrashort pulse width and the resulting ultrahigh laser light intensity in general.

When such ultrahigh intensity laser light interacts with the propagation medium, nonlinear optical effects (NLO effects) become significant. Typical NLO effects include NL refraction and NL absorption, and these effects are crucial phenomena to realize nanomachining or many other applications⁽⁵⁻⁷⁾. Nonlinear refraction leads to "Kerr effect" in which the refractive index strongly depends on the laser intensity and results in "self focusing" of the laser light. The nonlinear absorption, in which the absorption coefficient of the medium depends on laser intensity, results in "multiphoton ionization" or "tunnel ionization" to induce "laser-induced plasma" in ultrahigh intensity cases⁽⁸⁾. The laser-induced plasma causes "plasma defocusing" of laser light and "plasma absorption".

One of the most remarkable applications of NLO effects is 3D nanomachining in transparent media. By irradiating ultrashort pulse laser light to transparent medium, NL absorption takes place only at high intensity region and can fabricate microfluidics channels or micro waveguides in transparent media⁽⁶⁾⁽⁹⁾. These applications are very promising because they can be applied to integrated optics, telecommunications, sensors, lab-on-a-chip, MEMS and many more advanced devices to be fabricated in transparent media like glasses,

crystals and polymers. Theoretical approach, as well as experimental investigations, is very important to fully understand the complicated mechanisms in order to develop and commercialize such techniques.

In order to calculate the propagation of laser pulse, there are two major computational approaches: Beam Propagation Method (BPM) and Finite-Difference Time Domain (FDTD) method. BPM is more widely used because of its smaller calculation cost, and BPM-based short pulse laser propagation analysis can handle both nonlinear refraction and absorption⁽¹⁰⁻¹¹⁾. However, only a few existing FDTD-based models consider nonlinear absorption⁽¹²⁻¹³⁾ as far as the authors' knowledge, and these models do not consider the tunnel ionization effect and cylindrical coordinate is not dealt. It should be noted that BPM cannot be applied due to its "Slowly Varying Envelope Approximation" (SVEA) breakdown⁽¹⁴⁾ under ultrashort pulse width (typically several tens of femtoseconds or shorter) and the resulting small number of the wave numbers in the pulse envelope. In SVEA, backward wave and, in general, the third or higher order dispersions are neglected. Calculations by using BPM-based model therefore do not correctly describe the propagation of the pulse width of several tens of femtoseconds or shorter. It is also noted that the phase shift at the focal region⁽¹⁵⁾ of laser beam in general suggests the importance of solving the wave nature of the pulse propagation. The FDTD-based model, thus, must be developed and employed in order to fully describe the essential features of the phenomena.

In short pulse width cases in which the pulse width is much longer than that of the ultrashort pulse cases so that the SVEA does apply, BPM-based theoretical model is well-developed by comparing experimental evidences and it considers nonlinear refraction, absorption and laser-induced plasma⁽¹¹⁾. Therefore the knowledge associated with the NLO model is useful to develop FDTD-based model with NLO effects.

In this paper we develop a numerical model and to calculate short pulse laser propagation by using FDTD method. In this calculation the well-developed model in BPM is applied to develop FDTD-based model. In the model, NL absorption and the effect of the laser-induced plasma are considered. The results are examined by comparing with experiments and BPM-based calculations. It is also applied in ultrashort pulse case to investigate its propagation characteristics.

2. Nomenclature

- B : magnetic flux density, T
- H : magnetic field, A/m
- D : electric flux density, C/m^2
- E : electric field, V/m
- I : intensity of laser light, W/m^2
- ϵ_0 : electric permeability in vacuum, F/m
- μ_0 : magnetic permeability in vacuum, H/m
- c_0 : speed of light in vacuum, m/sec
- e : elementary charge, C
- n_0 : refractive index of medium
- σ : electric conductivity, S/m
- U_i : ionization energy of medium, J
- λ : wavelength of laser light, m
- ω : frequency of laser light, Hz
- k : wavenumber of laser light, m^{-1}
- $\chi^{(1)}$: linear susceptibility
- $\chi^{(3)}$: third-order nonlinear susceptibility, m^2/V^2
- w : laser beam radius, m
- t_p : pulse width, sec

f : focal length of lens, m

3. Numerical simulations of short laser pulse

3.1 Theory

In this paper, a Body of revolution (BOR) FDTD method⁽¹⁶⁾ is developed with the added ability the nonlinear effect as Kerr effect, multiphoton absorption and plasma defocusing⁽¹¹⁾. The BOR FDTD technique is derived starting from Maxwell's curl equations, following Eqs. (1a)–(1d):

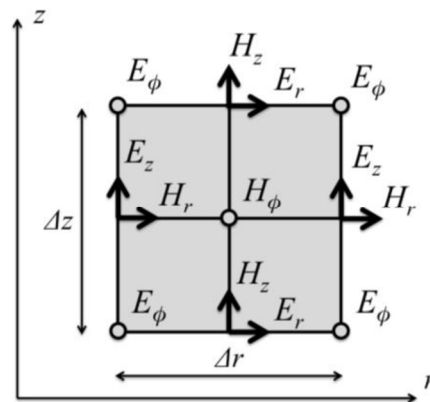
$$\text{div}B = 0 \tag{1a}$$

$$\text{div}D = 0 \tag{1b}$$

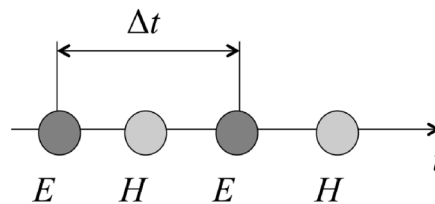
$$\text{rot}E + \frac{\partial B}{\partial t} = 0 \tag{1c}$$

$$\text{rot}H - \frac{\partial D}{\partial t} = \sigma E \tag{1d}$$

Schematic diagram of BOR FDTD is shown in Fig. 1. The axis of rotational symmetry is the z axis. Electric field $\mathbf{E}(E_r, E_\phi, E_z)$ and magnetic field $\mathbf{H}(H_r, H_\phi, H_z)$ propagating in the z direction shown in Fig. 1 where r and ϕ are beam radial and azimuthal direction, respectively.



(a) spatial domain



(b) time domain

Fig. 1 2D FDTD mesh used to represent the 3D field components in the axially symmetric formulation

The first step of this scheme is to calculate magnetic field \mathbf{H} from Eq. (1c). In cylindrical coordinate, Eq. (1c) is rewritten as

$$\begin{aligned} \mu_0 \left(\frac{\partial H_r}{\partial t} \hat{r} + \frac{\partial H_\phi}{\partial t} \hat{\phi} + \frac{\partial H_z}{\partial t} \hat{z} \right) = \\ - \left\{ \left(\frac{1}{r} \frac{\partial E_z}{\partial \phi} - \frac{\partial E_\phi}{\partial z} \right) \hat{r} + \left(\frac{\partial E_r}{\partial z} - \frac{\partial E_z}{\partial r} \right) \hat{\phi} + \left(\frac{1}{r} \frac{\partial (rE_\phi)}{\partial r} - \frac{1}{r} \frac{\partial E_r}{\partial \phi} \right) \hat{z} \right\} \end{aligned} \quad (2)$$

\mathbf{E} and \mathbf{H} are represented in terms of Fourier series expansion:

$$\begin{aligned} E_\zeta(r, \phi, z, t) &= \sum_{k=0}^{\infty} (E_{\zeta k 1}(r, z, t) \cos(k\phi) + E_{\zeta k 2}(r, z, t) \sin(k\phi)) \\ H_\zeta(r, \phi, z, t) &= \sum_{k=0}^{\infty} (H_{\zeta k 1}(r, z, t) \cos(k\phi) + H_{\zeta k 2}(r, z, t) \sin(k\phi)) \end{aligned} \quad (3)$$

where subscript ζ denotes r, ϕ and z . $E_{\zeta k 1}, E_{\zeta k 2}, H_{\zeta k 1}$ and $H_{\zeta k 2}$ are Fourier coefficients⁽¹⁶⁾. In this case, linearly polarized laser light is considered, and for a normally incident wave of only $k = 1$ mode is needed that is valid for our case. Considering both odd and even functions with regard to ϕ , Eq. (3) is written as

$$\begin{pmatrix} E_r \\ E_\phi \\ E_z \end{pmatrix} = \begin{pmatrix} E_{r1} \cos \phi \\ E_{\phi 1} \sin \phi \\ E_{z1} \cos \phi \end{pmatrix}, \quad \begin{pmatrix} H_r \\ H_\phi \\ H_z \end{pmatrix} = \begin{pmatrix} H_{r1} \sin \phi \\ H_{\phi 1} \cos \phi \\ H_{z1} \sin \phi \end{pmatrix} \quad (4)$$

where, subscripts of Fourier coefficients denoted by 1 and 2 are implied e.g. E_{r1} denotes $E_{r1 1}$. By substituting Eq. (4) into Eq. (2), we obtain

$$\begin{aligned} \mu_0 \left(\frac{\partial H_{r1}}{\partial t} \hat{r} + \frac{\partial H_{\phi 1}}{\partial t} \hat{\phi} + \frac{\partial H_{z1}}{\partial t} \hat{z} \right) = \\ \left(\frac{1}{r} E_{z1} + \frac{\partial E_{\phi 1}}{\partial z} \right) \hat{r} + \left(-\frac{\partial E_{r1}}{\partial z} + \frac{\partial E_{z1}}{\partial r} \right) \hat{\phi} + \left(-\frac{1}{r} \frac{\partial (rE_{\phi 1})}{\partial r} - \frac{1}{r} E_{r1} \right) \hat{z} \end{aligned} \quad (5)$$

Discretization of Eq. (5) is written as

$$\begin{aligned} H_{r1}^n(i, j+0.5) &= H_{r1}^{n-1}(i, j+0.5) + \frac{\Delta t}{\mu_0(i\Delta r)} E_{z1}^{n-0.5}(i, j+0.5) \\ &\quad + \frac{\Delta t}{\mu_0\Delta z} [E_{\phi 1}^{n-0.5}(i, j+1) - E_{\phi 1}^{n-0.5}(i, j)] \\ H_{\phi 1}^n(i+0.5, j+0.5) &= H_{\phi 1}^{n-1}(i+0.5, j+0.5) \\ &\quad - \frac{\Delta t}{\mu_0\Delta z} [E_{r1}^{n-0.5}(i+0.5, j+1) - E_{r1}^{n-0.5}(i+0.5, j)] \\ &\quad + \frac{\Delta t}{\mu_0\Delta r} [E_{z1}^{n-0.5}(i+1, j+0.5) - E_{z1}^{n-0.5}(i, j+0.5)] \\ H_{z1}^n(i+0.5, j) &= H_{z1}^{n-1}(i+0.5, j) \\ &\quad - \frac{\Delta t}{\mu_0[(i+0.5)\Delta r]} E_{r1}^{n-0.5}(i+0.5, j) - \frac{\Delta t}{\mu_0[(i+0.5)\Delta r]} \\ &\quad \times \frac{1}{\Delta r} \{ [(i+1)\Delta r] E_{\phi 1}^{n-0.5}(i+1, j) - [i\Delta r] E_{\phi 1}^{n-0.5}(i, j) \} \end{aligned} \quad (6)$$

where i and j are integer indexes ($0 \leq i \leq i_{max}, 0 \leq j \leq j_{max}$) along r and z axis, respectively. Here, magnetic field \mathbf{H}^n at the time step of n can be obtained. However on axis ($i = 0$) H_r cannot be obtained from Eq. (6). This boundary condition is given later.

The next step is to obtain plasma electron density ρ where evolution equation is written

as

$$\frac{\partial \rho}{\partial t} = W_{PI} + \frac{s}{U_i} \rho I - \frac{\rho}{\tau_r} \quad (7)$$

On the Right Hand Side (RHS) of Eq. (7), W_{PI} denotes Keldysh's formation⁽¹⁷⁾ for the photon ionization (PI) rate. The "Keldysh's parameter" is defined as $\gamma = \omega_0 \sqrt{m U_i} / e |E|$ where $m = 0.635 m_e$ denotes the reduced mass of the electron and the hole. W_{PI} approaches the tunnel formula for strong fields $\gamma \ll 1$, and the multiphoton rate for weak fields $\gamma \gg 1$. W_{PI} leads:

$$W_{PI}(|E|) = \frac{2\omega}{9\pi} \left(\frac{\omega m}{\hbar \sqrt{\Gamma}} \right)^{3/2} Q(\gamma, X) \exp(-\alpha \langle X+1 \rangle) \quad (8)$$

where,

$$\Gamma = \frac{\gamma^2}{1+\gamma^2}, \quad \Xi = \frac{1}{1+\gamma^2}, \quad X = \frac{2U_i K_2(\sqrt{\Xi})}{\hbar \omega \pi \sqrt{\Gamma}}, \quad \alpha = \pi \frac{K_1(\sqrt{\Gamma}) - K_2(\sqrt{\Gamma})}{K_2(\sqrt{\Xi})}, \quad \beta = \frac{\pi^2 K_2(\sqrt{\Xi})}{2K_1(\sqrt{\Xi})},$$

$$v = \langle X+1 \rangle - X, \quad Q(\gamma, X) = \sqrt{\frac{\pi}{2K_1(\sqrt{\Xi})}} \sum_{n=0}^{\infty} \exp(-n\alpha) \Phi(\sqrt{\beta(n+2v)})$$

$\langle \dots \rangle$ denote the integer part, K_1 and K_2 denote the complete elliptic integral of the first and second kind, and Φ denotes the Dawson function which is $\Phi(z) = \int_0^z \exp(y^2 - z^2) dy$. Figure 2 shows the ionization rate W_{PI} for silica as a function of the laser intensity. Dotted curve and dash-dotted curve denote Keldysh's multi-photon rate and tunnel ionization rate respectively. For weak fields, Keldysh's theory coincides with the six photon ionization rate $W_{MPI} \propto I^6$ (dashed line).

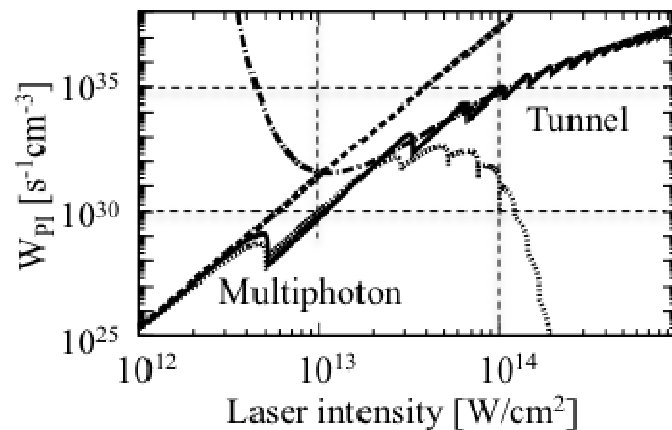


Fig. 2 Ionization rate for fused silica ($U_i = 9$ eV). This figure shows Keldysh's theory (solid line), the tunnel (dash-dotted line), multiphoton (dotted line), and six photon absorption rate $W_{MPI} \propto I^6$ (dashed line).

In the second term on RHS of Eq. (7), s denotes the cross section for inverse bremsstrahlung from the Drude model⁽¹⁸⁾ and is written as

$$s = \frac{ke^2}{n_0^2 \omega^2 \epsilon_0 m} \frac{\omega \tau_c}{(1 + \omega^2 \tau_c^2)} \quad (9)$$

where the momentum transfer collision time $\tau_c = 2.33 \times 10^{-14}$ s. In the third term on RHS of Eq. (7), τ_r denotes electron recombination with a characteristic time of $\tau_r = 150$ fs for fused silica⁽¹⁹⁾. Although τ_r is reported to depend on electric field, it is treated as a constant value in this paper.

We consider ρ as a uniform value over a unit cell, and it is evaluated at center of the cell. Thus, the discretization of Eq. (7) is written as

$$\begin{aligned} \rho^{n+0.5}(i+0.5, j+0.5) = & \left\{ 2W_{pl}^n(i+0.5, j+0.5)\Delta t \right. \\ & \left. + \left[2 - \Delta t \left(\frac{1}{\tau_r} - \frac{s}{U_i} I^n(i+0.5, j+0.5) \right) \right] \rho^{n-0.5}(i+0.5, j+0.5) \right\} / \\ & \left[2 + \Delta t \left(\frac{1}{\tau_r} - \frac{s}{U_i} I^n(i+0.5, j+0.5) \right) \right] \end{aligned} \quad (10)$$

where amplitude of electric field in a unit cell is needed to calculate ρ , and it is written as

$$\begin{aligned} |E(i+0.5, j+0.5)| &= \left[\left(\frac{E_{r1}(i+0.5, j) + E_{r1}(i+0.5, j+1)}{2} \cos \phi \right)^2 \right. \\ &+ \left(\frac{E_{\phi1}(i, j) + E_{\phi1}(i+1, j) + E_{\phi1}(i, j+1) + E_{\phi1}(i+1, j+1)}{4} \sin \phi \right)^2 \\ &\left. + \left(\frac{E_{z1}(i, j+0.5) + E_{z1}(i+1, j+0.5)}{2} \cos \phi \right)^2 \right]^{0.5} \end{aligned} \quad (11)$$

The next step is to obtain linear polarization P . To precisely describe Group Velocity Dispersion (GVD) we apply Sellmeier's formation to FDTD method⁽²⁰⁾ which has three linear polarizations P_m ($m = 1, 2, 3$) of that evolution equations are written as

$$\ddot{P}_{\zeta m} + \omega_m^2 P_{\zeta m} = \omega_m^2 b_m (\varepsilon_0 E_{\zeta}) \quad (m=1, 2, 3) \quad (12)$$

where parameters are $b_1 = 0.6961663$, $b_2 = 0.4079426$, $b_3 = 0.8974794$, $\lambda_1 = 0.0684043 \mu\text{m}$, $\lambda_2 = 0.1162414 \mu\text{m}$, $\lambda_3 = 9.896161 \mu\text{m}$ in fused silica⁽²⁰⁾ and $\omega_m = 2\pi c/\lambda_m$. Equation (12) is discretized as

$$P_{\zeta 1m}^{n+0.5} = (2 - \omega_m^2 \Delta t^2) P_{\zeta 1m}^{n-0.5} - P_{\zeta 1m}^{n-1.5} + \Delta t^2 \omega_m^2 b_m \varepsilon_0 E_{\zeta 1m}^{n-0.5} \quad (13)$$

The next step is to obtain \mathbf{D} and \mathbf{E} by using Eq. (1d). In a cylindrical coordinate system Eq. (1d) is rewritten as

$$\begin{aligned} \left[\left(\frac{\partial D_{r1}}{\partial t} + \sigma E_{r1} \right) \hat{r} + \left(\frac{\partial D_{\phi1}}{\partial t} + \sigma E_{\phi1} \right) \hat{\phi} + \left(\frac{\partial D_{z1}}{\partial t} + \sigma E_{z1} \right) \hat{z} \right] = \\ \left(\frac{1}{r} H_{z1} - \frac{\partial H_{\phi1}}{\partial z} \right) \hat{r} + \left(\frac{\partial H_{r1}}{\partial z} - \frac{\partial H_{z1}}{\partial r} \right) \hat{\phi} + \left(\frac{1}{r} \frac{\partial (rH_{\phi1})}{\partial r} - \frac{1}{r} H_{r1} \right) \hat{z} \end{aligned} \quad (14)$$

Equation (14) is discretized as

$$\begin{aligned}
 F_{r1}^{n+0.5}(i+0.5, j) &= G_{r1}^{n-0.5}(i+0.5, j) \\
 &+ \left[\frac{\Delta t}{(i+0.5)\Delta r} H_{z1}^n(i+0.5, j) - \frac{\Delta t}{\Delta z} [H_{\phi 1}^n(i+0.5, j+0.5) - H_{\phi 1}^n(i+0.5, j-0.5)] \right] \\
 F_{\phi 1}^{n+0.5}(i, j) &= G_{\phi 1}^{n-0.5}(i, j) \\
 &+ \frac{\Delta t}{\Delta z} [H_{r1}^n(i, j+0.5) - H_{r1}^n(i, j-0.5)] - \frac{\Delta t}{\Delta r} [H_{z1}^n(i+0.5, j) - H_{z1}^n(i-0.5, j)] \\
 F_{z1}^{n+0.5}(i, j+0.5) &= G_{z1}^{n-0.5}(i, j+0.5) - \frac{\Delta t}{(i\Delta r)} H_{r1}^n(i, j+0.5) \\
 &+ \frac{\Delta t}{(i\Delta r)} \frac{1}{\Delta r} \{ [(i+0.5)\Delta r] H_{\phi 1}^n(i+0.5, j+0.5) - [(i-0.5)\Delta r] H_{\phi 1}^n(i-0.5, j+0.5) \}
 \end{aligned} \tag{15}$$

where

$$\begin{aligned}
 F_{\zeta 1}^{n+0.5} &= D_{\zeta 1}^{n+0.5} + \sigma^n(i+0.5, j+0.5) \Delta t E_{\zeta 1}^{n+0.5} / 2 \\
 G_{\zeta 1}^{n-0.5} &= D_{\zeta 1}^{n-0.5} - \sigma^n(i+0.5, j+0.5) \Delta t E_{\zeta 1}^{n-0.5} / 2
 \end{aligned} \tag{16}$$

and on axis ($i = 0$) E_ϕ and E_z cannot be obtained from Eq. (15). This boundary condition is given later. σ consists of absorption coefficients of photon-ionization α_{PI} and plasma α_{plasma} which are written as

$$\sigma^n = 2\varepsilon_0 n_0 c_0 (\alpha_{PI}^n + \alpha_{plasma}^n) \tag{17}$$

$$\alpha_{PI}^n = \frac{W_{PI}^n U_i}{I^n} \tag{18}$$

$$\alpha_{plasma}^n = \frac{S}{2} \rho^n = \frac{S}{4} (\rho^{n+0.5} + \rho^{n-0.5}) \tag{19}$$

$F^{n+0.5}$ is used to obtain $E^{n+0.5}$.

To obtain $E^{n+0.5}$, we apply relational expression between D and E which is written as

$$D = \varepsilon_0 E + \sum_{m=1}^3 P_m + \varepsilon_0 \chi_{plasma} E + \varepsilon_0 \chi^{(3)} E^3 \tag{20}$$

where χ_{plasma} denotes specific permittivity of plasma which term describes effect of plasma defocusing and is written as

$$\chi_{plasma}(i_{pla}, j_{pla}) = -\frac{\tau_c^2}{1 + \omega^2 \tau_c^2} \frac{e^2}{m \varepsilon_0} \rho(i+0.5, j+0.5) \tag{21}$$

We can obtain $E^{n+0.5}$ by solving Eq. (21) substituting Eq. (16) with regard to $E^{n+0.5}$

$$\varepsilon_0 \chi^{(3)} (E_\zeta^{n+0.5})^3 + \varepsilon_0 \left(1 + \chi_{plasma} + \frac{\sigma^n \Delta t}{2} \right) E_\zeta^{n+0.5} + \left(\sum_{m=1}^3 P_{\zeta m}^{n+0.5} - F_\zeta^{n+0.5} \right) = 0 \tag{22}$$

Above all is the algorithm to simulate laser light propagation under nonlinear coupling by using FDTD. In our calculation, sizes of spatial and time steps (Δr , Δz and Δt) are restricted by

$$\sqrt{\Delta r^2 + \Delta z^2} \geq \frac{\lambda}{N} \tag{23}$$

where N should generally be 20 or greater. These step sizes are also restricted by CFL condition

$$\Delta t \leq \frac{1}{nc_0} \left\{ \frac{1}{\Delta r^2} \left[\frac{(k+1)^2 + 2.8}{4} \right] + \frac{1}{\Delta z^2} \right\}^{-1/2} \quad (24)$$

and by Eq. (7).

3.2 Boundary condition and Excitation source

On axis ($i = 0$) boundary condition of E_ϕ , E_z and H_r are written as

$$E_\phi(0, j) = 0, \quad E_z(0, j + 0.5) = 0, \quad H_r(0, j + 0.5) = 0 \quad (25)$$

At $i = i_{max}$, $j = 0$, j_{max} absorbing boundary condition (ABC) is Perfect Matched Layer (PML).⁽²¹⁾ In this PML medium, components of $\mathbf{E}(E_r, E_\phi, E_z)$ and $\mathbf{H}(H_r, H_\phi, H_z)$ are split into two subcomponents respectively : $\mathbf{E}(E_{r\phi}, E_{rz}, E_{\phi z}, E_{\phi r}, E_{zr}, E_{z\phi})$, $\mathbf{H}(H_{r\phi}, H_{rz}, H_{\phi z}, H_{\phi r}, H_{zr}, H_{z\phi})$. In this method \mathbf{H} is calculated from Eq. (1c) and written as

$$\begin{aligned} & \left(\mu_0 \frac{\partial H_{r\phi 1}}{\partial t} \right) \hat{r} + \left(\mu_0 \frac{\partial H_{\phi z 1}}{\partial t} + \sigma_{pml_z}^* H_{\phi z 1} \right) \hat{\phi} \\ & + \left(\mu_0 \frac{\partial H_{zr 1}}{\partial t} + \sigma_{pml_r}^* H_{zr 1} \right) \hat{z} = \left(\frac{1}{r} (E_{zr 1} + E_{z\phi 1}) \right) \hat{r} \\ & + \left(-\frac{\partial (E_{r\phi 1} + E_{rz 1})}{\partial z} \right) \hat{\phi} + \left(-\frac{1}{r} \frac{\partial [r (E_{\phi r 1} + E_{\phi z 1})]}{\partial r} \right) \hat{z} \end{aligned} \quad (26a)$$

$$\begin{aligned} & \left(\left(\mu_0 \frac{\partial H_{rz 1}}{\partial t} + \sigma_{pml_z}^* H_{rz 1} \right) \hat{r} + \left(\mu_0 \frac{\partial H_{\phi r 1}}{\partial t} + \sigma_{pml_r}^* H_{\phi r 1} \right) \hat{\phi} \right) \\ & + \left(\mu_0 \frac{\partial H_{z\phi 1}}{\partial t} \right) \hat{z} = \left(\frac{\partial (E_{\phi r 1} + E_{\phi z 1})}{\partial z} \right) \hat{r} \\ & + \left(\frac{\partial (E_{zr 1} + E_{z\phi 1})}{\partial r} \right) \hat{\phi} + \left(-\frac{1}{r} (E_{r\phi 1} + E_{rz 1}) \right) \hat{z} \end{aligned} \quad (26b)$$

where $\sigma_{pml_r}^*$ and $\sigma_{pml_z}^*$ are “magnetic loss” of PML medium which are explained later.

To obtain \mathbf{E} , \mathbf{D} is calculated from Eq. (1d) and written as

$$\begin{aligned} & \left(\frac{\partial D_{r\phi 1}}{\partial t} \right) \hat{r} + \left(\frac{\partial D_{\phi z 1}}{\partial t} + \sigma_{pml_z} E_{\phi z 1} \right) \hat{\phi} \\ & + \left(\frac{\partial D_{zr 1}}{\partial t} + \sigma_{pml_r} E_{zr 1} \right) \hat{z} = \left(\frac{1}{r} (H_{zr 1} + H_{z\phi 1}) \right) \hat{r} \\ & + \left(\frac{\partial (H_{r\phi 1} + H_{rz 1})}{\partial z} \right) \hat{\phi} + \left(\frac{1}{r} \frac{\partial [r (H_{\phi r 1} + H_{\phi z 1})]}{\partial r} \right) \hat{z} \end{aligned} \quad (27a)$$

$$\begin{aligned} & \left(\frac{\partial D_{rz 1}}{\partial t} + \sigma_{pml_z} E_{rz 1} \right) \hat{r} + \left(\frac{\partial D_{\phi r 1}}{\partial t} + \sigma_{pml_r} E_{\phi r 1} \right) \hat{\phi} \\ & + \left(\frac{\partial D_{z\phi 1}}{\partial t} \right) \hat{z} = \left(-\frac{\partial (H_{\phi r 1} + H_{\phi z 1})}{\partial z} \right) \hat{r} \\ & + \left(-\frac{\partial (H_{zr 1} + H_{z\phi 1})}{\partial r} \right) \hat{\phi} + \left(-\frac{1}{r} (H_{r\phi 1} + H_{rz 1}) \right) \hat{z} \end{aligned} \quad (27b)$$

where σ_{pml_r} and σ_{pml_z} are electric conductivity of PML medium which are explained later, and we apply relational equation between D and E in PML medium⁽²²⁾

$$D = \epsilon_0 E + \sum_{m=1}^3 P_m - \sum_{m=1}^3 P_m^{pml} \quad (28)$$

where P^{pml} is linear polarization derived from PML condition

$$P_m^{pml} = \epsilon_0 \left[\frac{b_m \sigma_{pml}}{\epsilon_0 (1 + b_1 + b_2 + b_3)} \frac{\omega j}{\omega_m^2 - \omega^2} \right] E \quad (29)$$

By transforming Eq. (30) to time domain,

$$\ddot{P}_{\epsilon 1 m}^{pml} + \omega_m^2 P_{\epsilon 1 m}^{pml} = \frac{b_m \sigma_{pml}}{\epsilon_0 (1 + b_1 + b_2 + b_3)} (\epsilon_0 \dot{E}_{\epsilon 1}) \quad (30)$$

is obtained and E can be calculated.

In PML condition σ_{pml} and σ_{pml}^* are written as

$$\begin{aligned} \sigma_{pml} &= \left[-\frac{(N+1)\epsilon_0 c}{2L\Delta\zeta} \ln|R| \right] \left(\frac{d}{L} \right)^N \\ \sigma_{pml}^* &= \frac{\mu_0}{\epsilon_0 (1 + b_1 + b_2 + b_3)} \sigma_{pml} \end{aligned} \quad (31)$$

where we set parameters as $N = 3$, number of layers $L = 50$ and reflection coefficient $R = 10^{-5}$. d is the number of layers from the boundary. Image of PML is shown in Fig. 3.

Excitation source is assumed as focused and linear polarized laser light which profile is temporally and spatially Gaussian and written as

$$E_{r1}^{n+0.5} = E_{source}^{n+0.5}, \quad E_{\phi 1}^{n+0.5} = -E_{source}^{n+0.5} \quad (32)$$

where

$$E_{source}^{n+0.5} = E_0 e^{-\frac{r^2}{w^2}} e^{-\frac{(t-2t_p)^2}{t_p^2}} \sin\left(\omega t + \frac{kr^2}{2f}\right) \quad (33)$$

In this case excitation source is considered as hard source, which does not allow transmission of wave through excitation source itself.

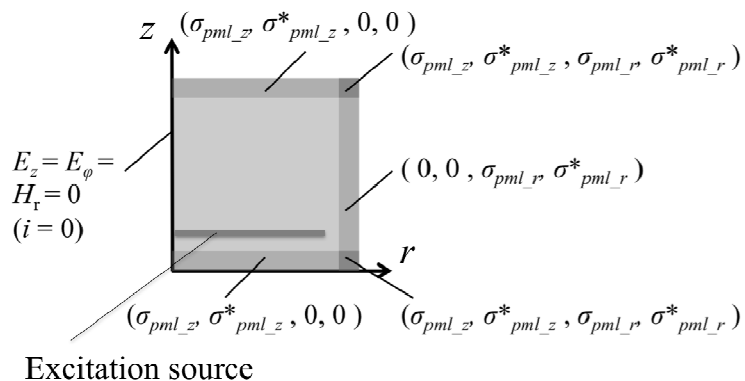


Fig. 3 Boundary condition and excitation source setting

3.3 Numerical condition

In order to examine FDTD-based calculation, the Gaussian fs-pulse propagation in silica in the high-power regime, where the power of the incident pulse is from several tens to several hundreds of times higher than P_{cr} of the glass, is simulated. First, the code is examined in regime of several tens times of P_{cr} by comparing with analytical results. We use an extension of Marburger's formula⁽²³⁾ which has been proposed in a Kerr medium without dispersion and plasma defocusing effect. In this case, the position of the nonlinear focal points are shown to be closely reproduced by

$$z_{NL} = z_0 / (\chi_M + z_0 / f) \quad (35)$$

where

$$z_0 = \pi w^2 n_0 / \lambda_0, \quad \chi_M = \frac{1}{0.367} \sqrt{\left(\left(\frac{P_m}{P_{cr}} \right)^{1/2} - 0.852 \right)^2 - 0.0219} \quad (36)$$

Here P_m indicates local maximum power in the temporal slice and P_{cr} denotes critical power of self focusing which is written as

$$P_{cr} = \frac{2\pi n_0 n_2}{\lambda_0^2} \quad (37)$$

In the higher power regime, several hundreds times of P_{cr} , this code is compared with the BPM-based results and experiment results in Ref. (11). FDTD-based numerical condition follows a BPM-based short pulse propagation analysis⁽¹¹⁾. Calculation system is shown in Fig. 4. In this system, short pulse laser focused by convex lens is irradiated to fused silica. Calculation is started at point of 100 μm from the focal point and calculate laser light propagation.

Parameters of laser and properties of medium are shown in Table 1. In this system Ti:Sapphier fs laser is considered and third order susceptibility $\chi^{(3)}$ is estimated by nonlinear refractive index $n_2 = 3.54 \times 10^{-16} \text{ cm}^2/\text{W}$.⁽¹¹⁾

In this study, furthermore, we calculate ultrashort pulse laser propagation under the condition as shown in Fig. 4 and table 2 by varying the momentum collision time of plasma τ_c , because pulse laser propagation dependence on τ_c has not been fully investigated so far. Momentum collision time of plasma τ_c are shown in table 2, where the reciprocal of frequency $1/\omega$ is 2.676 fs at wavelength of 800 nm.

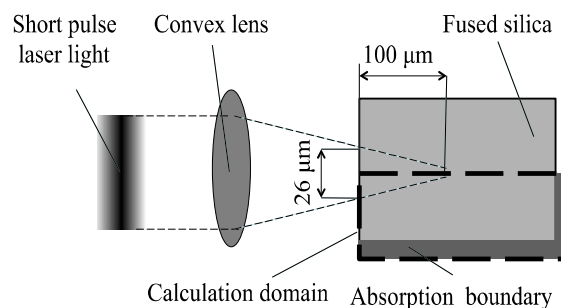


Fig. 4 A schematic of computational domain

Table 1. Numerical condition for short pulse analysis

Laser parameters	
Wavelength in air	800 nm
Pulse width (13.5% width)	272 fs
Beam diameter on surface	26 μm
Pulse energy per pulse	1.1 μJ
Property of medium	
n_0	1.45
$\chi^{(3)}$	$1.97 \times 10^{-22} \text{ m}^2/\text{V}^2$
U_i	9.0 eV

Table 2. Numerical condition for short and ultrashort pulse analysis

Laser parameters	
Momentum transfer collision time τ_c	$1/10\omega, 1/\omega, 10/\omega$
Pulse width (13.5% width)	$10/\omega$
Wavelength in air	800 nm
Pulse width (13.5% width)	272 fs
Beam diameter on surface	26 μm
Pulse energy per pulse	1.1 μJ

4. Numerical results of short laser pulse

Figure 5 shows numerical and analytical values of nonlinear focal length⁽²³⁾ without dispersion and plasma defocusing effect. Here focal point of lens is 50 μm from the surface, and linear dispersion and nonlinear absorption are neglected. Other conditions are as same as Fig. 4. Numerical results show a good agreement with the Marburger's formula⁽²³⁾ in regime of several tens times of P_{cr} .

Figure 6 show the beam radius for the fractions 13.5, 23.5, 33.5 and 43.5 % of radial peak fluence $F(z)$ and plasma electron density distribution $\rho(r,z)$. In Fig. 6 (a), focal length is shorter than that of lens. Therefore laser beam is strongly focused by Kerr effect. And around the focal point laser beam is defocused by the plasma and can be observed in Fig. 6 (b). Table 3 shows beam radius R_{FDTD} of FDTD-based result and R_{BPM} of BPM-based result, and Table 4 shows plasma radius for 10^{24} m^{-3} r_{FDTD} of FDTD-based result and r_{BPM} of BPM-based result. From both results show good agreements of FDTD-based results with those of BPM and the experimental results in Ref. (11). Therefore, the present FDTD-based model shows identical characteristics of propagation to BPM-based and experimental results.

Fig. 7 shows plasma electron density distribution for pulse width of $1/\omega = 27$ fs. In this ultrashort pulse case, plasma splitting occurs. This splitting is occurred by interference be-

tween focusing and strong plasma-defocused laser light. The same phenomenon can be observed in BPM simulation in short pulse and ultrahigh power case⁽²⁴⁾ and experiment⁽²⁵⁾. Here it should be denoted that this phenomena essentially depends on not pulse width but input power.

These results show that the present FDTD-based model can describe NLO effects and the essential features observed in experiment. As far as the authors' knowledge, it is the first time FDTD method succeeds to simulate the propagation of ultrafast pulse laser in several tens and hundreds times of P_{cr} .

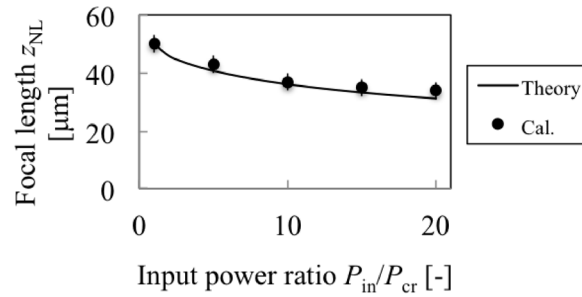
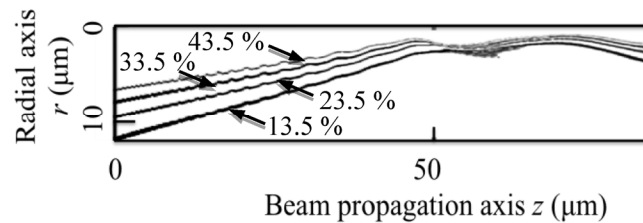
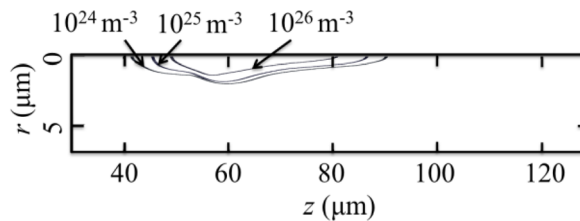


Fig. 5 Nonlinear focal length with no dispersion and no plasma



(a) Beam radius for the fractions 13.5, 23.5, 33.5 and 43.5 % of radial peak fluence $F(z)$



(b) Plasma electron density distribution

Fig. 6 Results of FDTD simulation

Table 3. Beam radius R comparison FDTD-based with BPM-based result

z [μm]	R_{BPM} [μm]	R_{FDTD} [μm]
21.56	7.77	7.92
52.87	3.077	3.076
59.13	3.84	3.84
68.53	2.42	2.50

Table 4. Radius of plasma r at 10^{24} m^{-3} comparison

FDTD-based with BPM-based result

z [μm]	r_{BPM} [μm]	r_{FDTD} [μm]
53	2.2	2.0
60	2.5	2.35
80	0.89	1.0

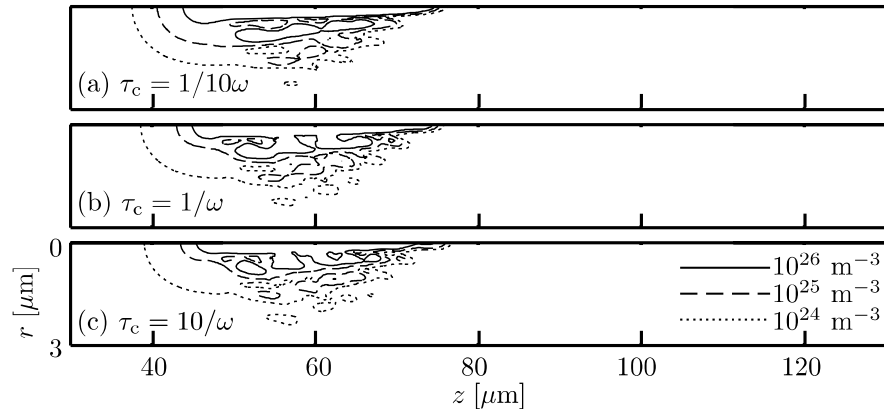


Fig. 7 Plasma electron density distribution for pulse width of 27 fs

5. Conclusion

In order to calculate the propagation of ultrashort pulse laser light in absorbing media, we have extended the existing FDTD model by employing the models in well-developed BPM-based model. In the present FDTD-based model, nonlinear absorption and the effect of laser-induced plasma are considered. Calculated results are examined by comparing with experiments, theory and BPM-based calculations. The calculated result of the present FDTD-based model exhibits identical characteristics of propagation to BPM-based, experimental and theoretical results and shows NLO effects by describing the essential features observed in experiment and theory.

Acknowledgement

Part of this work has been supported by the Grant-in-Aid for Scientific Research from MEXT/JSPS.

References

- (1) Stix, M. S., and E. P. Ippen; Pulse-shaping in passively mode-locked ring dye lasers, *IEEE Journal of Quantum Electronics*, Vol. 19, No. 4, (1983), pp.520-525.
- (2) S. De Silvestri, P. Laporta and O. Svelto; The role of cavity dispersion in CW mode-locked lasers, *IEEE Journal of Quantum Electronics*, Vol. 20, No. 5, (1984), pp.533-539.
- (3) N. Karasawa, L. Li, A. Suguro, H. Shigekawa, R. Morita and M. Yamasita; Optical pulse compression to 5.0 fs using only a spatial light modulator, *J. Opt. Soc. Am. B*, Vol. 18, No. 11, (2001), pp.1742-1746.
- (4) K. Yamane, Z. Zhang, K. Oka, R. Morita, M. Yamasita and A. Suguro; Optical pulse compression to 3.4 fs in the monocycle region by feedback phase compensation, *Opt. Lett.*, Vol. 28, No. 22, (2003), pp.2258-2260.

- (5) R. R. Gattass and E. Mazur; Femtosecond laser micro-machining in transparent materials, *nature photonics*, Vol. 2, (2008), pp.219-225.
- (6) F. He, Y. Cheng, Z. Xu, Y. Liao, J. Xu, H. Sun, C. Wang, Z. Zhou, K. Sugioka, K. Midorikawa, Y. Xu and X. Chen; Direct fabrication of homogeneous microfluidic channels embedded in fused silica using a femtosecond laser, *Opt. Lett.*, Vol. 35, No. 3, (2010), pp.282-284.
- (7) S. D. Borson, A. Kazeroonian, J. S. Moodera, D. W. Face, T. K. Cheng, E. P. Ippen, M. S. Dresselhaus and G. Dresselhaus; Femtosecond room-temperature measurement of the electron-phonon coupling constant γ in metallic superconductors, *Phys. Rev. Lett.*, Vol. 64, No. 18, (1990), pp.2172-2175.
- (8) E. Esarey, C. B. Schroeder and W. P. Leemans; Physics of laser-driven plasma-based electron accelerators, *Rev. Mod. Phys.*, Vol. 81, (2009), pp.1229-1285.
- (9) C. R. Mendonca, L. R. Cerami, T. Shih, R. W. Tilghman, T. Baldacchini and E. Mazur; Femtosecond laser waveguide micromachining of PMMA films with azaromatic chromophores, *Opt. Exp.*, Vol. 16, No. 1, (2008), 200-206.
- (10) A. Dubietis, A. Couairon, E. Kucinskas, G. Tamosauskas, E. Gaizauskas, D. Faccio, P. Di Trapani; Measurement and calculation of nonlinear absorption associated with femtosecond filaments in water, *Appl. Phys. B*, Vol. 84, (2006), pp.439-446.
- (11) A. Couairon, L. Sudrie, M. Franco, B. Prade and A. Mysyrowicz; Filamentation and damage in fused silica induced by tightly focused femtosecond laser, *Appl. Phys. B*, Vol. 71, (2005), pp.125435.
- (12) I. B. Bogatyrev, D. Grojo, P. Delaporte, S. Leyder, M. Sentis, W. Marine and T. E. Itina; Non-linear absorption of 1.3- μm wavelength femtosecond laser pulses focused inside semiconductors: Finite difference time domain-two temperature model combined computational study, *J. Appl. Phys.*, Vol. 110, (2011), pp.103106.
- (13) N. Suzuki; FDTD Analysis of Two-Photon Absorption and Free-Carrier Absorption in Si High-Index-Contrast Wave-guides, *J. Lightwave Tech*, Vol.25, No. 9, (2007), pp.2495-2501.
- (14) S. Nakamura, T. Saeki and Y. Koyamada; Observation of Slowly Varying Envelope Approximation Breakdown by Comparison between the Extended Finite-Difference Time-Domain Method and the Beam Propagation Method for Ultrashort-Laser-Pulse Propagation in a Silica Fiber, *J. Appl. Phys.* Vol. 43, No. 10, (2004), pp.7015-7025.
- (15) C. R. Gouy; On a new property of light waves (in French), *C. R. Acad. Sci. Paris*, Vol. 110, (1890), pp.1251-1253.
- (16) D. B. Davidson and R. W. Ziolkowski, Body-of-revolution finite-difference time-domain modeling of space-time focusing by a three-dimensional lens; *J. Opt. Soc. Am. A*, Vol. 11, No. 4, (1994), pp.1471-1490.
- (17) L. V. Keldysh, Ionization in the field of a strong electromagnetic wave, *Sov. Phys.*, Vol. 20, (1965), pp.1307-1314
- (18) B. C. Stuart, M. D. Feit, S. Herman, A. M. Rubenchik, B. W. Shore and M. D. Perry; Nanosecond-to-femtosecond laser-induced breakdown in dielectrics, *Phys. Rev. B*, Vol. 53, No. 4, (1996), pp.1749-1761.
- (19) P. Audebert, Ph. Daguzan, A. Dos Santos, J. C. Gauthier, J. P. Geindre, S. Guizard, G. Hamoniaux, K. Krastev, P. Martin, G. Petite and A. Antonetti; Space-Time Observation of an Electron Gas in SiO_2 , *Phys. Rev. Lett.* Vol. 73, No. 14, (1994), pp.1990-1993.
- (20) S. Nakamura, N. Takasawa, Y. Koyamada, H. Sone, L. Xu, R. Morita and M. Yamasita; Extended Finite Difference Time Domain Analysis of Induced Phase Modulation and Four-Wave Mixing between Two-Color Femtosecond Laser Pulses in a Silica Fiber with Different Initial Delays, *J. Appl. Phys.*, Vol. 44, No. 10, (2005), pp.7453-7459.
- (21) Y. Liu, Z. Lu, Z. Ren, F. Li and Z. Cao; Perfectly matched layer absorbing boundary conditions in rigorous vector analysis of axially symmetric diffractive optical elements (in Japanese), *Optics Communications*, Vol. 223, (2003), pp.39-45.
- (22) T. Uno and S Kojima; Berenger-type PML Absorbing Boundary Condition for Frequency-dependent Material, *Tech. Report of IEICE*, Vol. 96, No. 149, (1996), pp.27-33.
- (23) J. H. Marburger; Self-focusing: Theory, *Progress in Quantum Electronics*, Vol. 4, (1975), pp.35-110.

- (24) K. Ishikawa, H. Kumagai, and K. Midorikawa; High-power regime of femtosecond-laser pulse propagation in silica: multiple-cone formation, *Phys. Rev. E*, Vol. 66, Issue 5, (2002), pp.056608.1-056608.8
- (25) H. Kumagai, S. Cho, K. Ishikawa, K. Midorikawa, M. Fujimoto, S. Aoshima, and Y. Tsuchiya; Observation of the complex propagation of a femtosecond laser pulse in a dispersive transparent bulk material, *J. Opt. Soc. Am. B*, Vol. 22, No. 3, (2003), pp.597-602